The Relationship of the Clinical Disc Margin and Bruch's Membrane Opening in Normal and Glaucoma Subjects

Navid Amini, Arezoo Miraftabi, Sharon Henry, Norman Chung, Sarah Nowroozizadeh, Joseph Caprioli, and Kouros Nouri-Mahdavi

Glaucoma Imaging Research Laboratory, Stein Eye Institute, David Geffen School of Medicine, University of California, Los Angeles, California, United States

Correspondence: Kouros Nouri-Mahdavi, 100 Stein Plaza, Los Angeles, CA 90095, USA; nouri-mahdavi@jsei.ucla.edu.

PURPOSE. We tested the hypotheses that the mismatch between the clinical disc margin (CDM) and Bruch's membrane opening (BMO) is a function of BMO area (BMOA) and is affected by the presence of glaucoma.

METHODS. A total of 45 normal eyes (45 subjects) and 53 glaucomatous eyes (53 patients) were enrolled and underwent radial optic nerve head (ONH) imaging with spectral domain optical coherence tomography. The inner tip of the Bruch's membrane (BM) and the clinical disc margin were marked on radial scans and optic disc photographs, and were coregistered with custom software. The main outcome measure was the difference between the clinical disc area (CDA) and BMOA, or CDA−BMOA mismatch, as a function of BMOA and diagnosis. Multivariate regression analyses were used to explore the influence of glaucoma and BMOA on the mismatch.

RESULTS. Global CDA was larger than BMOA in both groups but the difference was statistically significant only in the normal group (1.98 ± 0.37 vs. 1.85 ± 0.45 mm², $P = 0.02$ in the normal group; 1.96 ± 0.38 vs. 1.89 ± 0.56 mm², $P = 0.08$ in the glaucoma group). The sectoral CDA−BMOA mismatch was smaller in superotemporal ($P = 0.04$) and superonasal ($P = 0.05$) sectors in the glaucoma group. The normalized CDA−BMOA difference decreased with increasing BMOA in both groups ($P < 0.001$). Presence or severity of glaucoma did not affect the CDA−BMOA difference ($P > 0.14$).

CONCLUSIONS. Clinical disc area was larger than BMOA in normal and glaucoma eyes but reached statistical significance only in the former group. The CDA−BMOA mismatch diminished with increasing BMOA but was not affected by presence of glaucoma. These findings have important clinical implications regarding clinical evaluation of the ONH.

Keywords: glaucoma, spectral-domain OCT, Bruch's membrane opening, clinical disc margin, RNFL

Glaucoma is a chronic optic neuropathy characterized by slow loss of the retinal ganglion cells (RGC) and their axons. Early damage to RGC axons is considered to occur at the level of the lamina cribrosa (LC), a multilayered connective tissue structure through which all the RGC axons pass when leaving the eye to form the optic nerve.[1] Hence, studying the anatomy of the optic nerve head (ONH) and the peripapillary area is important for studying the mechanisms by which glaucoma damages these structures. Historically, the inner edge of the sclera, called the border tissue of Elschnig, has been presumed to form the clinical optic disc margin or outer boundary of the anterior neural canal. The complex relationships of the tissues bordering the neural canal now is better understood thanks to availability of in vivo imaging of the peripapillary region with spectral domain optical coherence tomography (SD-OCT). Strouthidis et al.[2] recently proposed that the appearance of the clinical disc margin depended mainly on the colocation of the inner edge of the Bruch's membrane (BM) and the border tissue of Elschnig (BTE). The direction of the BTE has been shown to vary around the ONH and internally oblique, externally oblique, and nonoblique configurations have been well defined.[3,4]

The termination of the BM around the optic nerve forms the BM opening (BMO), which defines the anterior most boundary of the neural canal and commonly is the narrowest part of the neural canal. In monkeys, the clinical disc margin consistently localizes to BMO,[3,5] while based on findings by Reis et al.,[6] this is not the case in humans. In human eyes, BM overhang (i.e., extension of BM beyond the BTE) is common. The BMO area may better predict the number of ganglion cell axons in individual eyes or indicate the best location for centering SD-OCT's disc/retinal nerve fiber layer (RNFL) measurement cube,[7] although it is likely that the narrowest region of the neural canal determines the axonal complement of a given eye. In addition, it has been demonstrated that neuroretinal rim area measurements based on the minimum distance between the inner edge of BMO and the internal limiting membrane (minimum rim width [MRW]) are superior to those based on clinical disc margin (horizontal rim width).[8] Also, MRW measurements have been found to perform better or at least as well as peripapillary RNFL thickness measurements for discriminating glaucoma from normal eyes and demonstrate similar structure–function relationships compared to RNFL.[8,9]

1468

To date, most clinical disc area measurements are based on identification of the clinical disc margin by experienced observers either on optic disc photographs or on images obtained with scanning laser ophthalmoscopy (such as the Heidelberg Retina Tomograph [HRT]). Some of the current SD-OCT machines have an automated algorithm for locating the inner edge of the BMO. Whether the relationship between the BMO and the clinical disc margin (CDM) is a function of the size of the optic disc is unknown; likewise, it is unclear whether BMO area can change over time in glaucoma.

This study was performed to test the hypothesis that the anatomical relationship of the CDM and BMO is a function of the BMO area (BMOA). We also tested the hypothesis that the relationship between the clinical disc margin and BMO was different between glaucoma and normal eyes with less mismatch in glaucoma eyes.

METHODS

Normal subjects were enrolled prospectively as part of ongoing studies at the Glaucoma Imaging Research Laboratory of the University of California, Los Angeles (UCLA). Furthermore, a group of glaucoma patients from the Advanced Glaucoma Progression Study (AGPS) were enrolled in the study. Details of the AGPS methods have been published previously.[10-12] All studies were approved by the Institutional Review Board at UCLA and were performed in adherence with the Declaration of Helsinki.

Study Subjects

Patients diagnosed with open-angle glaucoma by an attending physician at the Stein Eye Institute's Glaucoma Clinic and who met the following criteria were enrolled prospectively in the study: age ≥ 30 years, open angles, visual acuity $\geq 20/80$, refractive error ≤ 8.0 diopters (D) and astigmatism ≤ 3 D. The perimetric criteria for selecting AGPS eyes is as follows: visual field mean deviation ≤ -6 dB, or better than -6.0 dB as long as at least 2 points of the 12 test locations located within the central $10°$ of the 24-2 visual fields demonstrated a P value of $<5\%$ on pattern deviation plot. Eyes with evidence of any disc anomaly including any signs of disc tilt or disc torsion, such as vertically or obliquely oval disc, presence of temporal crescent of atrophy, or significant sloping of the temporal neuroretinal rim compared to other sectors, based on qualitative review of stereoscopic disc photograph by one of the investigators (KNM), were excluded. Also, eyes with other significant ocular disorders or neurological diseases were not enrolled. All patients had at least one prior visual field test before being enrolled in the study.

Normal subjects were recruited by advertising on UCLA's campus and soliciting spouses or friends of patients seen at Stein Eye Institute's Glaucoma Clinics. The enrolled normal subjects were required to have open angles, corrected visual acuity of 20/25 or better, a normal eye exam including normal visual fields, and no definitive evidence of glaucomatous damage at the level of the ONH as well as no evidence of disc anomalies as detailed above for glaucoma eyes.

All subjects underwent a full eye exam on the day of imaging, which included visual acuity, automated refraction, IOP measurement, gonioscopy, slit-lamp exam, dilated fundus exam, and standard achromatic perimetry (SAP). An IOLMaster (Carl Zeiss-Meditec, Dublin CA, USA) was used to measure axial length. Stereoscopic optic disc photographs and ONH scans (Spectralis; Heidelberg Engineering, Heidelberg, Germany) were done after pupillary dilation.

Glaucoma was diagnosed if a reproducibly abnormal SAP visual field was present and was consistent with the optic disc findings. An abnormal SAP visual field was defined as presence of a Glaucoma Hemifield Test (GHT) outside normal limits and presence of ≥ 4 abnormal test locations on the pattern deviation plot with $P < 5\%$, both confirmed at least once.[13] The Swedish Interactive Thresholding Algorithm (SITA) standard testing strategy was used. Reliable visual fields were defined as those with a false-positive rate of $\leq 20\%$. The visual fields were reviewed to exclude lid or lens artifacts.

Imaging Methods

Retinal nerve fiber layer (RNFL) and ONH imaging was done with Spectralis SD-OCT (software version 5.3). A radial scanning pattern centered on the ONH was used to obtain 24 B-scans. The scans were angularly equidistant (i.e., $15°$ B-scans) with 768 A-scans in each B-scan. The RNFL imaging included a $12°$ circular scan composed of 768 A-scans centered on the ONH. In addition to the global RNFL thickness (G), the RNFL thickness in six sectors: nasal (N, $135°-225°$), superonasal (NS, $90°-135°$), superotemporal (TS, $45°-90°$), temporal (T, $315°-45°$), inferotemporal (TI, $270°-315°$), and inferonasal (NI, $225°-270°$), in the clockwise direction for the right eye and counterclockwise direction for the left eye were exported by the Spectralis into a personal computer.

For each eye, an experienced clinician (AM) marked the inner BMO edges on each of the 24 B-scans. The same clinician (AM) also determined the presence of BM overhang on a separate session. Radial scans where the BMO extended beyond the Border Tissue of Elschnig were considered to have a BM overhang. The CDM was delineated on the optic disc photographs by a different experienced clinician (SN) while viewing the stereo disc photograph pairs on a computer monitor with a stereo viewer (Screen Vu; PS Mfg, Venice, CA, USA) as defined by Reis et al.[6] Figures 1A and 1B provide examples to demonstrate that what is perceived by the clinician as the clinical disc margin can vary from eye to eye depending on the interplay of the RPE, inner choroidal layers, and the BM/BTE complex. For example, in Figure 1B, the end of the RPE (red arrows) or choroidal pigment (white arrows) could be mistaken for the CDM. Figure 1C demonstrates an example of a tilted disc where the edge of the BM actually is visible temporally on clinical exam outside what is perceived to be the clinical disc margin. A subgroup of 20 eyes was selected randomly from normal and glaucoma groups (10 eyes per group) and the CDM marked by a different clinician (KNM) to assess the reproducibility of CDM demarcation. A custom MATLAB program (ver. 8.1; MathWorks, Cambridge, MA, USA) was used to project the location of the inner tip of BMO marked on individual B-scans onto infrared en face SD-OCT images (Fig. 2). The infrared images and optic disc photographs were registered (overlaid) with a generalized dual bootstrap iterative closest point algorithm with i2k retina software (DualAlign LLC, Clifton, NY, USA).[14] In this way, the location of the BMO edge with regard to CDM could be evaluated (Fig. 2).

Area measurements were calculated for BMO and clinical disc area (CDA) after registering the marked optic disc images with en face infrared images of the optic disc. Such measurements were performed for global CDA and BMOA as well as six sectors as defined by Spectralis (see above). The BMO/CDM offset, defined as the distance between the centroids of BMO and the CDM, also was calculated. To convert measurements in pixels to measurements in millimeters, individual mm-to-pixel ratios generated by the Spectralis software were used. Such ratios are used by the device to correct for the optical magnification of the eye and are based
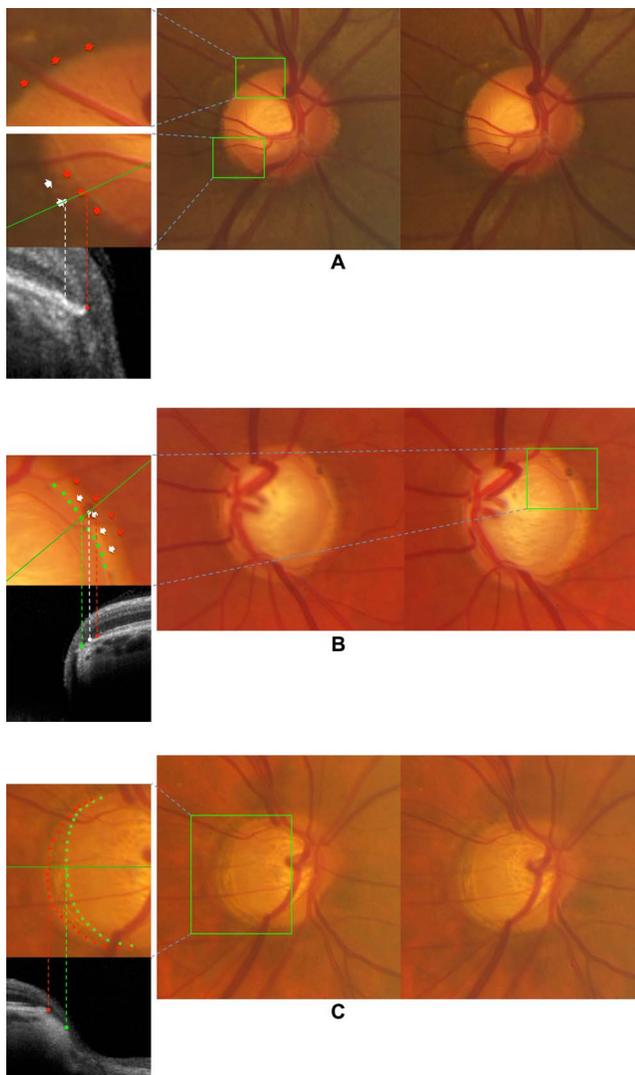
FIGURE 1. Various examples of the appearance of the clinical disc margin demonstrate that its visibility is influenced by the interplay between peripapillary tissues. (**A**) The structure considered to be the disc margin is well demarcated due to the RPE extending all the way to the neuroretinal rim and the strong color contrast between the two. Superotemporally (*top inset*), neither BM inner edge nor the BTE is visible due to the dense pigmentation of the RPE, whereas inferotemporally (*middle inset*), the RPE shows various degrees of atrophy and the well-defined structure identified as the disc margin is formed by the BM and underlying BTE. *Inset, bottom*: SD-OCT B-scan along the *green line* demonstrates the correspondence between the clinical and OCT findings. (**B**) Stereoscopic photographs of an eye with advanced glaucoma and extensive peripapillary atrophy. *Inset*: The RPE (*red arrows*) and deeper pigmented choroidal layers (*white arrows*) stop short of the disc margin (*green dots*), which is seen here as the innermost extension of the BTE/BM complex. *Inset, bottom*: The SD-OCT B-scan along the *green line* shows the correspondence between the clinical and OCT findings. (**C**) Stereoscopic photographs of a moderately tilted glaucomatous disc where the BM is clearly visible (*inset, red dots*) outside of the clinical disc margin (*inset, green dots*). The clinically observed disc margin represents part of the BTE. *Inset, bottom*: Horizontal SD-OCT B-scan of the same eye (along the *green line*) demonstrates the correspondence between clinical and OCT findings in the temporal region. Eyes with any degrees of tilt as observed clinically on stereoscopic exam of the disc were excluded from this study.

on each eye's corneal curvature, which are entered before imaging, and the focusing mechanism of the device as a proxy for the axial length.[15]

The Spectralis software provides an RNFL printout that includes average and sectoral RNFL thickness measurements as well as color-coded comparison to an age-matched normative database for the RNFL thickness. Thickness values that fall within the normal range are classified as within normal limits ($P > 5\%$, coded by green color), while thickness values that fall outside the normal range for the age are either considered borderline ($P < 5\%$ and $\geq 1\%$, coded by yellow color) or outside normal limits ($P < 1\%$, coded by a red color). Abnormality levels of RNFL thickness were gathered from Spectralis RNFL printouts to compare evidence of RNFL loss (i.e., glaucomatous damage) in sectors with and without BM overhang.

Evaluation of Reproducibility of Clinical Disc Margin Marking

To assess the reproducibility of CDM delineation, a second experienced clinician (KNM) marked the clinical disc margin on the optic disc photographs for a subgroup of 20 eyes as mentioned above. Coordinates of the marked points were saved for comparison against the demarcation of the CDM by the first clinician. For each eye, we calculated the spatial overlap between the optic disc regions (namely, R_1 and R_2) delimited by the two clinicians. To quantify the extent of overlap, the Jaccard Index (JI),[16–18] defined as the size of the intersection divided by the size of the union, was used:

$$JI(R_1, R_2) = \frac{\text{Area}(R_1 \cap R_2)}{\text{Area}(R_1 \cup R_2)}.$$

The *JI* of 1 means that the two regions are identical and have complete overlap and the *JI* of 0 represents no overlap between the two regions.

Statistical Methods

Only one eye from each subject was included. The main outcome measures were CDM–BMO mismatch or the difference between CDA and BMOA as a function of BMO area and diagnosis. We examined various plots including frequency distribution, normal quantile, and polar plots, to explore the outcomes of interest. The Kolmogorov-Smirnov test was used to check for normality of the distribution of continuous variables. Wilcoxon rank-sum or *t*-test, as indicated, were used to compare such variables. Bruch's membrane overhang was compared in eyes with small and large BMOA after empirically dividing the eyes into 2 tiers based on the median BMOA in each group. We used multivariate regression analyses with backward variable entry to determine whether the difference in BMOA and CDA was a function of diagnosis after adjusting for potential confounding factors affecting the CDM-BMO mismatch, such as BMO size, axial length, BMO/CDM offset, and age. Variables with a *P* value <0.20 or variables that were thought to potentially affect the outcome were kept in the model. Categorical variables, such as the statistical significance of RNFL abnormality and the presence of BM overhang, were tabulated in $n \times m$ tables and compared with the χ^2 test. All analyses were done with the Stata software (version 12.1; StataCorp College Station, TX, USA).

RESULTS

We included in the current study 98 eyes of 98 subjects (53 eyes of 53 glaucoma patients and 45 eyes of 45 normal
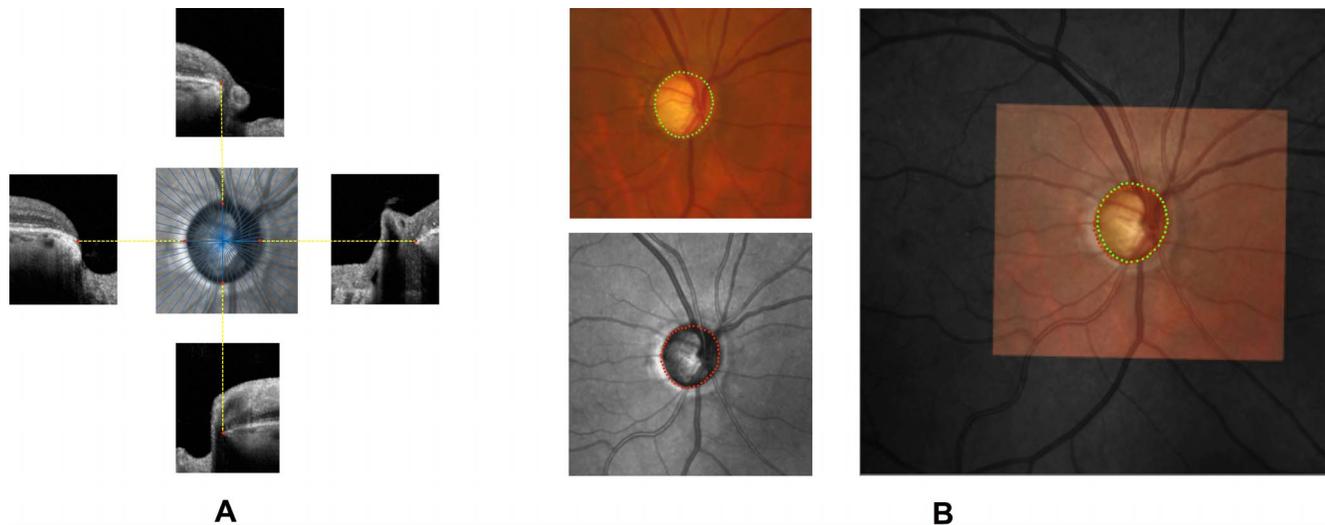
FIGURE 2. (A) En face infrared disc image from Spectralis SD-OCT (*center*) and portions of four radial SD-OCT B-scans. Bruch's membrane opening (BMO) was identified on the B-scans by a clinician (*red dots* on peripheral images). Location of the BMO was projected to en face image (*red dots* on the *central image*); (B) Colocalization of disc photographs with en face infrared images. Disc photograph of a glaucoma patient with optic disc area of 1.82 mm^2 (*top left*) is registered with its en face infrared (*bottom left*). The registered disc photograph was superimposed at 38% transparency on the en face image (*right panel*). Note the mismatch between the clinical disc margin (*green dots*) and the BMO (*red dots*).

subjects). Table 1 summarizes the clinical and demographic characteristics of the enrolled subjects. The mean ($\pm$SD) age was 53.7 ($\pm$13.9) years in the normal group and 69.0 ($\pm$9.0) years in the glaucoma patients ($P < 0.001$). The glaucoma patients had a longer axial length compared to normal subjects (median and interquartile range [IQR]: 24.1 [23.3–25.4] vs. 23.8 [22.8–24.5] mm, respectively; $P = 0.04$). Median and IQR of BMOA were 1.74 (1.54–2.15) and 1.77 (1.59–2.16) mm^2 in the normal and glaucoma groups, respectively ($P = 0.90$). Median and IQR of CDA were 1.92 (1.74–2.16) and 1.88 (1.74–2.20) mm^2 for the normal and glaucoma groups, respectively ($P = 0.92$). Average BMO/CDM offset was 13 ($\pm$1) pixels or 74 ($\pm$6) μm in the control group and 15 ($\pm$1) pixels or 87 ($\pm$5) μm in the glaucoma group ($P = 0.09$).

The average JI obtained by comparing the CDM demarcation by the two clinicians was 0.958 ($\pm$0.003), which indicates that the delineation of the CDM was highly reproducible. These results compare well with others reported in the literature.[18] It should be noted that fundus images in our study cohort had to be of sufficient quality to be included. The average JI in the glaucomatous eyes was slightly lower than that in the normal eyes (0.953 [$\pm$0.005] vs. 0.963 [$\pm$0.003]; $P = 0.12$).

Figure 3 illustrates the frequency distribution of the BMOA in the two groups. The BMOA was significantly smaller than CDA (1.87 $\pm$ 0.51 vs. 1.97 $\pm$ 0.37 mm^2; $P = 0.01$ in the entire

cohort), while the difference was statistically significant in the normal group (1.85 $\pm$ 0.45 vs. 1.98 $\pm$ 0.37 mm^2; $P = 0.02$), it did not reach statistical significance in the glaucoma group (1.89 $\pm$ 0.56 vs. 1.96 $\pm$ 0.38 mm^2; $P = 0.08$). The normal and glaucomatous eyes were divided into two groups as a function of the median BMOA (1.74 mm^2 for normal and 1.77 mm^2 for glaucomatous eyes). As the polar plots in Figure 4 indicate, a BM overhang was observed most commonly in the superonasal (86%), inferonasal (77%), inferotemporal (73%), and nasal (73%) sectors in normal eyes. In the glaucoma group, a BM overhang was most frequent in the inferonasal (85%), nasal (80%), and temporal (78%) sectors. There was no statistically significant relationship between occurrence of a BMO overhang in normal and glaucomatous eyes ($P > 0.1$ all sectors, χ^2 test). Furthermore, this relationship did not vary as a function of BMOA ($P > 0.22$ and $P > 0.11$, χ^2 test).

The main outcome of interest in our study was the difference between the CDA and BMOA. It was normalized with respect to BMOA to account for potential confounding introduced by the BMOA; that is, for the same amount of mismatch in BMO and CDM, larger discs would demonstrate a larger difference between the CDA and BMOA due to a larger circumference. The difference between the CDA and BMOA was a function of BMO ($P < 0.001$) for both groups, that is, the discrepancy between CDA and BMO tended to become smaller as the BMOA became larger after normalization relative to the

TABLE 1. Demographic and Clinical Characteristics of the Study Sample

Number (Subjects/Eyes)	Total (98/98)	Normal (45/45)	Glaucoma (53/53)	P Value
Age, y, mean ($\pm$SD)	62.0 ($\pm$13.8)	53.7 ($\pm$13.9)	69.0 ($\pm$9.0)	<0.001*
Sex, female/male	50/48	19/26	31/22	0.94†
Lens status, phakic/pseudophakic	76/22	44/1	32/21	<0.001†
Axial length, median, dB (IQR)	24.0 (23.0–24.7)	23.8 (22.8–24.5)	24.1 (23.3–25.4)	0.04‡
Mean deviation, median, dB (IQR)	−2.16 (−5.92−−0.34)	−0.14 (−0.95–0.13)	−5.55 (−12.03−−3.02)	<0.001‡
BMO area, median, mm^2 (IQR)	1.75 (1.55–2.16)	1.74 (1.54–2.15)	1.77 (1.59–2.16)	0.90‡
Clinical disc area, median, mm^2 (IQR)	1.91 (1.74–2.20)	1.92 (1.74–2.16)	1.88 (1.74–2.20)	0.92‡

* 2-sample *t*-test.
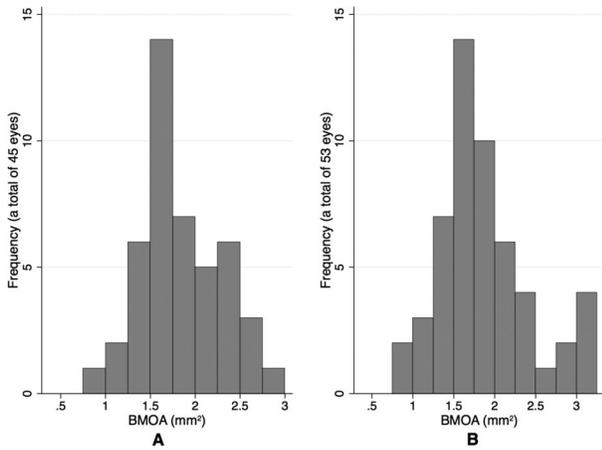† χ^2 test.
‡ Wilcoxon rank-sum test.

FIGURE 3. *Bar graph* shows the distribution of BMO area for (**A**) the normal eyes; (**B**) the glaucomatous eyes.

FIGURE 5. Scatter plot demonstrates the correlation between BMOA and clinical disc area mismatch as a function of the BMOA for the normal and glaucoma groups.

size of the BMO. The regression coefficients were −0.32 ($P < 0.001$; 95% CI, [−0.458–−0.228]) and −0.25 ($P < 0.001$; 95% CI, [−0.323–−0.187]) for the normal and glaucoma groups. The change in (CDA − BMOA) normalized for the BMOA as a function of BMOA is demonstrated in Figure 5 for normal and glaucomatous eyes. It can be observed that the magnitude of the mismatch between the CDM and BMO becomes smaller with increasing BMOA. The difference between sectoral CDA and BMOA was significantly smaller in the superotemporal (ST) and superonasal (SN) sectors in the glaucoma group ($P = 0.04$ for ST and $P = 0.05$ for SN). For all other sectors, the difference was not significant ($P > 0.24$).

We used multivariate linear regression analyses to determine potential factors affecting the CDM–BMO mismatch. Of particular interest was whether the CDM–BMO mismatch, expressed as CDA − BMOA, varied as a function of glaucoma diagnosis or severity. To this aim, two separate multivariate regression models were constructed with one including a diagnosis of glaucoma as a binary independent variable and the second one using the visual field mean deviation (MD) as an index for severity of glaucoma (Tables 2, 3). Other variables incorporated in both models included the BMOA, BMOA interaction with glaucoma, axial length, BMO/CDM centroid offset, and age. The results of both models were in agreement with regard to lack of an association between glaucoma and
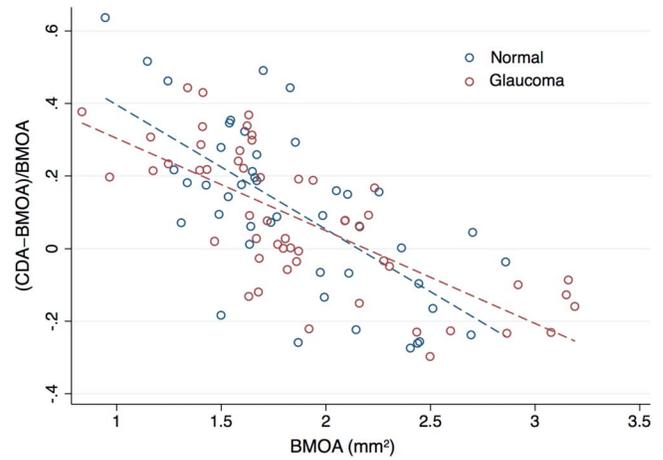
CDM–BMO mismatch ($P = 0.14$ and 0.31 for the first and second models, respectively). In both models, a smaller BMOA ($P < 0.001$) was associated with a larger mismatch. Age was not a predictor for CDM–BMO mismatch in either model ($P = 0.58$ and 0.49, respectively).

The association between the presence of a statistically abnormal RNFL thickness (defined according to the Spectralis normative database) and BM overhang was next investigated to explore whether presence of BMO overhang was associated with statistically thinner peripapillary RNFL measurements. Table 4 summarizes the results of bivariate cross-tabulation analysis of RNFL thickness abnormality level and BM overhang. There was no evidence of an association between BM overhang and RNFL abnormality either globally or sectorally ($P > 0.16$; χ^2 test) except in the inferonasal sector ($P = 0.02$).

DISCUSSION

Spectral-domain OCT has become the imaging device of choice for detecting presence of glaucoma or disease worsening, although solid data are scarce with regard to the latter task. Bruch's membrane opening, which can be detected with SD-OCT imaging, is the anterior most structure of the neural canal.
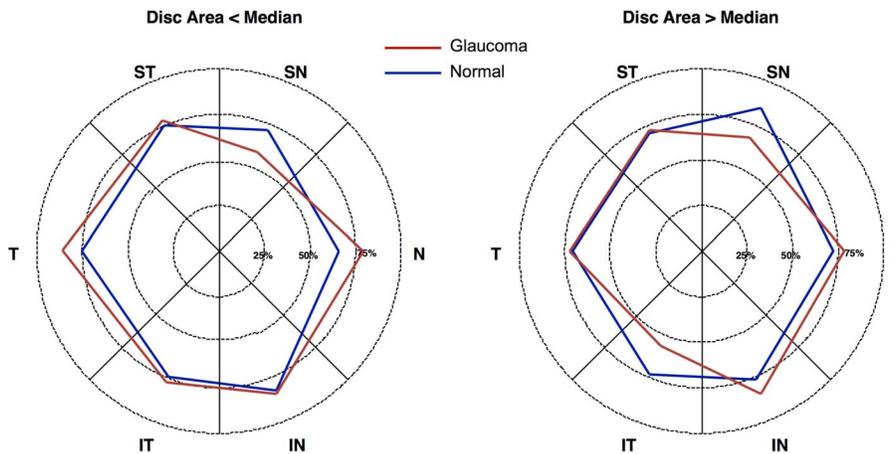

FIGURE 4. Frequency of BM/CDM mismatch by sectors for eyes with smaller BMO area (<1.74 and 1.77 mm² for normal and glaucoma eyes, respectively, *left panel*) and larger BMO area (>1.74 and 1.77 mm² for normal and glaucoma eyes, respectively, *right panel*). The distance from origin in each sector represents frequency of BMO/CDM mismatch.

TABLE 2. Results of a Multivariate Regression Analysis to Determine the Influence a of Diagnosis of Glaucoma on the Mismatch Between CDM and BMO With Glaucoma Entered as a Binary Variable Into the Model

CDA − BMOA/BMOA Variables	β	SE	P Value	(95% Confidence Interval)
Glaucoma, ref: normal	−0.188	0.128	0.14	(−0.441, 0.066)
BMOA, per mm²	−0.354	0.051	<0.001	(−0.456, −0.252)
Glaucoma × BMOA, per mm²	0.089	0.064	0.16	(−0.038, 0.216)
Age, per y	−0.001	0.001	0.58	(−0.004, 0.002)
Axial length, per mm	0.018	0.011	0.12	(−0.005, 0.040)
BMO/CDM centroid offset, per μm	<0.001	<0.001	0.32	(0, 0.001)

The main outcome of interest was the difference between CDA and BMO area normalized by the latter. β, regression coefficient.

TABLE 3. Results of a Multivariate Regression Analysis to Determine the Influence of Glaucoma Severity as Represented by Visual Field MD on the Mismatch Between CDM and BMO

CDA − BMOA/BMOA Variables	β	SE	P Value	95% Confidence Interval
Mean deviation, per dB	0.011	0.011	0.31	(−0.011, 0.033)
BMOA, per mm²	−0.323	0.045	<0.001	(−0.412, −0.234)
MD × BMOA, per dB*mm²	−0.005	0.005	0.38	(−0.015 0.006)
Age, per y	−0.001	0.001	0.49	(−0.003, 0.002)
Axial length, per mm	0.017	0.011	0.13	(−0.005, 0.039)
BMO/CDM centroid offset, per μm	<0.001	<0.001	0.33	(0, 0.001)

The main outcome of interest was the difference between CDA and BMO area normalized by the latter. β, regression coefficient.

There is a growing consensus that BMO may be a more consistent anatomic landmark compared to the clinical disc margin for measuring various ONH related parameters, such as the newly defined MRW[8,19,20] and minimum rim area.[8,21]

A number of current SD-OCT devices (such as Cirrus HD-OCT and Spectralis SD-OCT) have an automated algorithm for demarcating the inner edge of the BMO. An important clinical question is whether the relationship of the BMO with regard to the clinically defined optic disc margin is a function of the BMOA. In other words, does the mismatch between our clinical impression of the clinical disc margin and the BMO vary as a function of the BMO area? Since the location of BM is rarely visible on ophthalmoscopy in humans, the relationship of BMO and clinical disc margin should be explored with more sophisticated technology, such as SD-OCT. Other investigators and our group have shown previously a significant discrepancy between the SD-OCT disc area and HRT-derived or clinically determined disc size.[22,23] Our results showed that the CDM–BMO mismatch was less prominent globally in eyes with a larger BMOA. The global mismatch was not influenced by presence or severity of glaucoma regardless of the way it was entered in the multivariate models. When CDM–BMO mismatch was compared in ONH sectors, glaucoma eyes had less CDM–BMO mismatch in the superonasal and superotemporal quadrant. There was no significant association between age or axial length and the CDM–BMO mismatch. Interestingly, although the *P* values did not reach statistical significance, the regression coefficient was positive, probably indicative of the fact that longer eyes with tilted disc had been adequately excluded from the study sample.

Reis et al.[6] recently demonstrated that BM overhang is present commonly in human eyes, it is not visible in humans, and a combination of various BTE configurations frequently exists in normal and glaucomatous eyes with the externally oblique configuration most commonly observed inferiorly and temporally. These investigators also showed that the structure corresponding to the clinical disc margin in humans is not anatomically unique, and consists of a combination of the BMO edge and the inner border or some part of the BTE. Although internally oblique border tissue (with BM overhang) is the predominant configuration in most discs, in general, more than one border tissue configuration is present. It is possible that the location of glaucomatous optic disc damage also could be driven by the anatomic characteristics of the anterior neural canal, among other factors; one might hypothesize that presence of BMO overhang or specific BTE configurations could cause preferential axonal damage in glaucoma. We explored the association between these two parameters in sectors defined by Spectralis SD-OCT. We found that BM overhang was a frequent finding in normal and glaucoma eyes, observed in up to 86% of normal eyes and 85% of glaucoma eyes. This finding is consistent with that of Reis et al.[6] The proportion of sectors showing BM overhang was not statistically different between the normal and glaucoma groups except inferonasally ($P = 0.02$). Given the multiple comparisons performed and the borderline significance of this relationship, it is not clear whether this finding has any real biological significance. This issue must be explored in future studies. It is expected that automated delineation of BMO along with automatic registration of fundus photographs and en face infrared images of the optic disc will facilitate confirmation of our findings in future studies.

These results have significant clinical implications. The BMO has been considered a stable reference for disc-related measures and as mentioned, has been considered as a proxy for the disc area. Most optic disc and RNFL parameters, such as the rim area, cup volume, or cross-sectional RNFL area, are related to the disc area, although there is controversy about the latter association.[24,25] The fact that the relationship of CDM and BMO was a function of BMOA could be explained partially at least in eyes with smaller discs by the fact that in such eyes, the optic disc frequently has fairly indistinct margin and, therefore, the clinical disc margin may be considered and placed farther beyond the location of the BMO. Given the fact that clinicians estimate the neuroretinal rim thickness in relationship to the CDM, this could explain to some extent the finding that glaucomatous damage is less obvious in such eyes and is underestimated. We took meticulous care while marking the CDM so that for areas where the RPE or pigmented inner choroidal layers stopped short of the CDM, such transition zones were not erroneously marked as the CDM (Fig. 1B). Such peripapillary changes are more common in glaucoma and older subjects; a lack of an association between age and the CDM-BMO mismatch in both groups is reassuring. Reis et al.[6] suggested that the mismatch between BMO and the clinical disc margin might be affected by age. Johnstone et al.[26] recently demonstrated that peripapillary choroidal thickness was negatively correlated with age and that BMO height, measured relative to a scleral reference plane, was lower in older individuals. This was attributed to choroidal atrophy. Although BMO could possibly migrate posteriorly with age as a result of age-related choroidal thinning, longitudinal evidence for this observation has yet to be reported. The difference between the CDA and BMOA (CDA − BMOA normalized relative to the BMOA) was not related to age in our study ($P = 0.58$ and 0.49 for the normal and glaucomatous eyes).

TABLE 4. Bivariate Cross-Tabulation Analysis of RNFL Thickness Abnormality and BM Overhang

Abnormality of RNFL Thickness	Overhang, T	Overhang, TS	Overhang, NS	Overhang, N	Overhang, NI	Overhang, TI	Overhang, Combined
P >5%, green	43/63	39/53	53/72	57/77	53/70	41/55	286/390
1% < P <5%, yellow	16/19	5/8	7/12	10/14	18/18	1/3	57/74
P <1%, red	14/16	28/37	8/14	6/7	10/10	26/40	92/124
Total	73/98	72/98	68/98	73/98	81/98	68/98	435/588
χ^2 P cvalue	0.16	0.74	0.32	0.76	0.02	0.24	0.80

Abnormality of RNFL thickness is based on the normative database of Spectralis SD-OCT.

The CDM–BMO relationships may change as glaucoma progresses due to the constant trans-lamina cribrosa pressure gradient,[27] to which the BMO is exposed over years, and may lead to posterior bowing and possibly enlargement of the BMO. There is some evidence that the edge of BM can curve backward in glaucomatous eyes.[28] This could potentially affect the CDM–BMO mismatch, but as mentioned above, we did not find any strong supporting evidence in this cross-sectional study. If a change in BMO position with glaucoma progression is confirmed in future studies, the clinical implication is that BM movement with worsening glaucoma may make it a less than optimal reference for measuring disc-related structural parameters. A longitudinal change in BMO might affect MRW measurements despite no true loss in the axonal complement of an individual eye. This issue must be explored in future studies.

Eyes with tilted disc very frequently are myopic and the tilt is caused by the asymmetric expansion of the posterior pole[29] and temporal expansion of the BMO. In these eyes, the BMO frequently is located temporal to the clinically perceived disc margin and the BMOA is likely not well correlated with the axonal count of the optic nerve. Therefore, such eyes were excluded from this study. We considered the widely used criterion for defining a tilted disc (a tilt index or ratio of longest disc diameter to shortest disc diameter of 1.33 or more as described in previous studies[30–32]) too insensitive to be of use in this study. Another limitation of the current study is that the sample size was not adequate to explore the outcomes of interest in various ethnicities. There is evidence that the disc size varies across ethnicities.[33–35] Seider et al.[36] showed that Caucasian-American subjects had smaller optic discs than African-, Asian-, Hispanic-, and Filipino-Americans as measured by the HRT in a glaucoma clinic-based population.[36] The glaucoma patients investigated in this study were not age-matched with control subjects. However, based on multivariate analyses, age was not a predictor for CDM–BMO mismatch. Observation of a similar correlation between CDM–BMO mismatch and the BMOA for normal and glaucoma groups indicated that our findings should be generalizable ($P < 0.001$ for both groups).

No correction was applied for ocular magnification. The Spectralis software generates individual μm-to-pixel ratios based on each subject's corneal curvature to minimize the effects of ocular magnification.[15] Also, the focusing mechanism of the Spectralis SD-OCT machine corrects to some extent for the refractive error of individual eyes and, hence, adjusts for the effect of ocular magnification.[12,37] A comparison of the axial length between phakic and pseudophakic eyes showed that the difference between the mean axial lengths in the two groups was not significant (mean axial length, 24.02 vs. 24.25 mm; $P = 0.5$). It should be noted that ocular magnification would not affect pairwise comparisons of CDA and BMOA.

It now is believed that the axis connecting the foveal center to the BMO centroid (fovea–BMO axis) should be considered the reference axis for defining the origin of the RNFL TSNIT profile or that of the newly defined minimum width rim area.[8,21] We have shown recently that while performing RNFL analysis relative to such axis did not enhance glaucoma detection, it improved the prediction limits of RNFL in a number of sectors. In general, it is suggested that fovea–BMO axis in individual eyes should be used as the reference axis for regionalization of all ONH- and RNFL-related outcomes. We compared CDA and BMOA in sectors 45° to 90° in width. Therefore, regionalization with regard to the fovea–BMO axis would have minimally changed our results.

In summary, we found that the BMO area was on average smaller than clinical disc area; this finding was more pronounced in normal eyes compared to eyes with glaucoma. The difference between the two decreased as a function of BMO area in glaucomatous and normal eyes. There was no evidence of an association between BM overhang and statistically abnormal RNFL thickness in SD-OCT sectors. Future investigations should focus on relationships of clinical disc margin and BMO in various ethnicities and on longitudinal changes in the relationship between these two anatomical landmarks in normal and glaucoma subjects.

Acknowledgments

Disclosure: **N. Amini**, None; **A. Miraftabi**, None; **S. Henry**, None; **N. Chung**, None; **S. Nowroozizadeh**, None; **J. Caprioli**, Allergan (C, F), Heidelberg (F); **K. Nouri-Mahdavi**, Allergan (F), Heidelberg (F)

References

1. Quigley HA, Addicks EM, Green WR, Maumenee AE. Optic nerve damage in human glaucoma. II. The site of injury and susceptibility to damage. *Arch Ophthalmol*. 1981;99:635–649.

2. Strouthidis NG, Yang H, Fortune B, Downs JC, Burgoyne CF. Detection of optic nerve head neural canal opening within histomorphometric and spectral domain optical coherence tomography data sets. *Invest Ophthalmol Vis Sci*. 2009;50:214–223.

3. Strouthidis NG, Yang H, Downs JC, Burgoyne CF. Comparison of clinical and three-dimensional histomorphometric optic disc margin anatomy. *Invest Ophthalmol Vis Sci*. 2009;50:2165–2174.

4. Strouthidis NG, Yang H, Reynaud JF, et al. Comparison of clinical and spectral domain optical coherence tomography optic disc margin anatomy. *Invest Ophthalmol Vis Sci*. 2009;50:4709–4718.

5. Downs JC, Yang H, Girkin C, et al. Three-dimensional histomorphometry of the normal and early glaucomatous monkey optic nerve head: neural canal and subarachnoid space architecture. *Invest Ophthalmol Vis Sci*. 2007;48:3195–3208.

6. Reis AS, Sharpe GP, Yang H, Nicolela MT, Burgoyne CF, Chauhan BC. Optic disc margin anatomy in patients with glaucoma and normal controls with spectral domain optical coherence tomography. *Ophthalmology*. 2012;119:738–747.

7. Chung JK, Yoo YC. Correct calculation circle location of optical coherence tomography in measuring retinal nerve fiber layer thickness in eyes with myopic tilted discs. *Invest Ophthalmol Vis Sci*. 2011;52:7894–7900.

8. Chauhan BC, O'Leary N, Almobarak FA, et al. Enhanced detection of open-angle glaucoma with an anatomically accurate optical coherence tomography-derived neuroretinal rim parameter. *Ophthalmology*. 2013;120:535–543.

9. Danthurebandara VM, Sharpe GP, Hutchison DM, et al. Enhanced structure-function relationship in glaucoma with an anatomically and geometrically accurate neuroretinal rim measurement. *Invest Ophthalmol Vis Sci*. 2015;56:98–105.

10. Amini N, Nowroozizadeh S, Cirineo N, et al. Influence of the disc-fovea angle on limits of RNFL variability and glaucoma discrimination. *Invest Ophthalmol Vis Sci*. 2014;55:7332–7342.

11. Nouri-Mahdavi K, Nowroozizadeh S, Nassiri N, et al. Macular ganglion cell/inner plexiform layer measurements by spectral domain optical coherence tomography for detection of early glaucoma and comparison to retinal nerve fiber layer measurements. *Am J Ophthalmol*. 2013;156:1297–1307.e1292.

12. Nowroozizadeh S, Cirineo N, Amini N, et al. Influence of correction of ocular magnification on spectral-domain oct retinal nerve fiber layer measurement variability and performance. *Invest Ophthalmol Vis Sci*. 2014;55:3439–3446.

13. Johnson CA, Sample PA, Cioffi GA, Liebmann JR, Weinreb RN. Structure and function evaluation (SAFE): I. criteria for glaucomatous visual field loss using standard automated perimetry (SAP) and short wavelength automated perimetry (SWAP). *Am J Ophthalmol*. 2002;134:177–185.

14. Stewart CV, Tsai CL, Roysam B. The dual-bootstrap iterative closest point algorithm with application to retinal image registration. Vol 22. *IEEE Trans Med Imaging*. 2003;1379–1394.

15. Ctori I, Gruppetta S, Huntjens B. The effects of ocular magnification on Spectralis spectral domain optical coherence tomography scan length. *Graefes Arch Clin Exp Ophthalmol*. 2015;253:733–738.

16. Teussink MM, Breukink MB, van Grinsven MJ, et al. OCT Angiography compared to fluorescein and indocyanine green angiography in chronic central serous chorioretinopathy. *Invest Ophthalmol Vis Sci*. 2015;56:5229–5237.

17. Morales S, Naranjo V, Angulo U, Alcaniz M. Automatic detection of optic disc based on PCA and mathematical morphology. *IEEE Trans Med Imaging*. 2013;32:786–796.

18. Yu H, Barriga ES, Agurto C, et al. Fast localization and segmentation of optic disk in retinal images using directional matched filtering and level sets. *IEEE Trans Inf Technol Biomed*. 2012;16:644–657.

19. Reis AS, O'Leary N, Yang H, et al. Influence of clinically invisible, but optical coherence tomography detected, optic disc margin anatomy on neuroretinal rim evaluation. *Invest Ophthalmol Vis Sci*. 2012;53:1852–1860.

20. Cull GA, Reynaud J, Wang L, Cioffi GA, Burgoyne CF, Fortune B. Relationship between orbital optic nerve axon counts and retinal nerve fiber layer thickness measured by spectral domain optical coherence tomography. *Invest Ophthalmol Vis Sci*. 2012;53:7766–7773.

21. Gardiner SK, Ren R, Yang H, Fortune B, Burgoyne CF, Demirel S. A method to estimate the amount of neuroretinal rim tissue in glaucoma: comparison with current methods for measuring rim area. *Am J Ophthalmol*. 2014;157:540–549.e541.

22. Sharma A, Oakley JD, Schiffman JC, Budenz DL, Anderson DR. Comparison of automated analysis of Cirrus HD OCT spectral-domain optical coherence tomography with stereo photographs of the optic disc. *Ophthalmology*. 2011;118:1348–1357.

23. Moghimi S, Hosseini H, Riddle J, et al. Measurement of optic disc size and rim area with spectral-domain OCT and scanning laser ophthalmoscopy. *Invest Ophthalmol Vis Sci*. 2012;53:4519–4530.

24. Budenz DL, Anderson DR, Varma R, et al. Determinants of normal retinal nerve fiber layer thickness measured by Stratus OCT. *Ophthalmology*. 2007;114:1046–1052.

25. Huang D, Chopra V, Lu AT, et al. Does optic nerve head size variation affect circumpapillary retinal nerve fiber layer thickness measurement by optical coherence tomography? *Invest Ophthalmol Vis Sci*. 2012;53:4990–4997.

26. Johnstone J, Fazio M, Rojananuangnit K, et al. Variation of the axial location of Bruch's membrane opening with age, choroidal thickness, and race. *Invest Ophthalmol Vis Sci*. 2014;55:2004–2009.

27. Burgoyne C. The morphological difference between glaucoma and other optic neuropathies. *J Neuroophthalmol*. 2015;35(suppl 1):S8–S21.

28. Lee KY, Tomidokoro A, Sakata R, et al. Cross-sectional anatomic configurations of peripapillary atrophy evaluated with spectral domain-optical coherence tomography. *Invest Ophthalmol Vis Sci*. 2010;51:666–671.

29. Kim TW, Kim M, Weinreb RN, Woo SJ, Park KH, Hwang JM. Optic disc change with incipient myopia of childhood. *Ophthalmology*. 2012;119:21–26.e21.

30. How AC, Tan GS, Chan YH, et al. Population prevalence of tilted and torted optic discs among an adult Chinese population in Singapore: the Tanjong Pagar Study. *Arch Ophthalmol*. 2009;127:894–899.

31. Jonas JB, Kling F, Gründler AE. Optic disc shape, corneal astigmatism, and amblyopia. *Ophthalmology*. 1997;104:1934–1937.

32. Park KA, Park SE, Oh SY. Long-term changes in refractive error in children with myopic tilted optic disc compared to children without tilted optic disc. *Invest Ophthalmol Vis Sci*. 2013;54:7865–7870.

33. Patel NB, Lim M, Gajjar A, Evans KB, Harwerth RS. Age-associated changes in the retinal nerve fiber layer and optic nerve head. *Invest Ophthalmol Vis Sci*. 2014;55:5134–5143.

34. Knight OJ, Girkin CA, Budenz DL, Durbin MK, Feuer WJ. Group CONDS. Effect of race, age, and axial length on optic nerve head parameters and retinal nerve fiber layer thickness measured by Cirrus HD-OCT. *Arch Ophthalmol*. 2012;130:312–318.

35. Girkin CA, Sample PA, Liebmann JM, et al. African Descent and Glaucoma Evaluation Study (ADAGES): II. Ancestry differences in optic disc, retinal nerve fiber layer, and macular structure in healthy subjects. *Arch Ophthalmol*. 2010;128:541–550.

36. Seider MI, Lee RY, Wang D, Pekmezci M, Porco TC, Lin SC. Optic disk size variability between African, Asian, white, Hispanic, and Filipino Americans using Heidelberg retinal tomography. *J Glaucoma*. 2009;18:595–600.

37. Sanchez-Cano A, Baraibar B, Pablo LE, Honrubia FM. Magnification characteristics of the Optical Coherence Tomograph STRATUS OCT 3000. *Ophthalmic Physiol Opt*. 2008;28:21–28.